

Modeling of North Pacific Climate Variability Forced by Oceanic Heat Flux Anomalies

ELENA YULAEVA, NIKLAS SCHNEIDER, DAVID W. PIERCE, AND TIM P. BARNETT

Climate Research Division, Scripps Institution of Oceanography, University of California, San Diego, La Jolla, California

(Manuscript received 19 December 2000, in final form 23 April 2001)

ABSTRACT

Potential predictability of low-frequency climate changes in the North Pacific depends on two main factors. The first is the sensitivity of the atmosphere to ocean-induced anomalies at the sea surface in midlatitudes. The second is the degree of teleconnectivity of the tropical low-frequency variability to midlatitudes. In contrast to the traditional approach of prescribing sea surface temperature (SST) anomalies, the response of a coupled atmospheric general circulation (CCM3)-mixed layer ocean model to oceanic perturbations of the mixed layer heat budget is examined. Since positive oceanic heat flux perturbations partially increase SST anomalies (locally), and partially are vented directly into the atmosphere, expressing boundary forcing on the atmosphere by prescribing upper-ocean heat flux anomalies allows for better understanding of the physical mechanism of low-frequency variability in midlatitudes. In the framework of this approach SST is considered to be a part of the adjustment of the coupled system rather than an external forcing. Wintertime model responses to mixed layer heat budget perturbations of up to 40 W m^{-2} in the Kuroshio extension region and in the tropical central Pacific show statistically significant anomalies of 500-mb geopotential height (Z500) in the midlatitudes. The response to the tropical forcing resembles the well-known Pacific-North American pattern, one of the leading modes of internal variability of the control run. The amplitude of the Z500 geopotential height reaches 40 m in the region of the Aleutian low. The response of Z500 to forcing in the Kuroshio Current extension region resembles the mixture of western Pacific and Pacific-North American patterns, the first two modes of the internal variability of the atmosphere. In midlatitudes this response is equivalent barotropic, with the maximum of 80 m at (60°N, 160°W). Examination of the vorticity and thermodynamic budgets reveals the crucial role of submonthly transient eddies in maintaining the anomalous circulation in the free atmosphere.

At the surface the response manifests itself in changes of surface temperature and the wind stress. The amplitude of response to the tropical forcing in the SST field at the Kuroshio Current extension region is up to 0.3 K (in absolute value) that is 2 times weaker than SST anomalies induced by midlatitude forcing of the same amplitude. In addition, the spatial structures of the responses in the SST field over the North Pacific are different. While tropical forcing induces SST anomalies in the central North Pacific, the midlatitude forcing causes SST anomalies off the east coast of Japan, in the Kuroshio-Oyashio extension region. Overall, remote tropical forcing appears to be effective in driving anomalies over the central North Pacific. This signal can be transported westward by the oceanic processes. Thus tropical forcing anomalies can serve as a precursor of the changes over the western North Pacific.

In the case of midlatitude forcing, the response in the wind stress field alters Ekman pumping in such a way that the expected change of the oceanic gyre, as measured by the Sverdrup transport, would counteract the prescribed forcing in the Kuroshio extension region, thus causing a negative feedback. This response is consistent with the hypothesis that quasi-oscillatory decadal climate variations in the North Pacific result from midlatitude ocean-atmosphere interaction.

1. Introduction

Decadal climate variability over the North Pacific has important implications for climate prediction over North America since it is strongly related to atmospheric variability over the continent (e.g., Latif and Barnett 1996; Barnett et al. 1999; Livezey and Smith 1999), and modulates ENSO teleconnections to the region (Gershunov and Barnett 1998). Reliable forecasting of climate var-

iations over North America requires an understanding of the physical mechanism underlying changes in the North Pacific.

Ocean-atmosphere coupling in midlatitudes is of particular importance for prognostication of North American climate. Barnett et al. (1999) identified two main unresolved questions on the ocean-atmosphere coupling in midlatitudes: 1) what is the direct impact of the midlatitude upper-ocean anomalies on atmospheric variability? and 2) is there a feedback between the ocean and atmosphere that allows an existence of low-frequency oscillatory mode?

If the low-frequency climate change results from two-way interaction between the ocean and the atmosphere

Corresponding author address: Dr. Elena Yulaeva, Climate Research Division, Scripps Institution of Oceanography, University of California, San Diego, 9500 Gilman Drive, La Jolla, CA 92093-0224.
E-mail: eyulaeva@ucsd.edu

that involve delay due to ocean dynamics (Latif and Barnett 1994, 1996), then the process is potentially predictable, and sophisticated numerical modeling can dramatically improve the forecast skill over North America.

On the other hand, if the ocean integrates random atmospheric forcing (Hasselmann 1976; Barsugli and Battisti 1998; Bretherton and Battisti 2000) without significant feedback to the atmosphere, the benefit of dynamic climate modeling for long-lead forecasts for North America is marginal at best.

To resolve the question of the impact of midlatitude ocean anomalies on atmospheric variability, modeling studies are often used. The motivation for such extensive use of simulations may be explained by difficulty of separation “cause and effect” from observational data alone, since the ocean–atmosphere system is intrinsically coupled. The way in which the ocean anomalies are imposed in a modeling study [via sea surface temperature (SST) or heat flux anomalies] is important as these related but nonetheless distinct quantities affect the atmosphere differently.

The classic approach toward simulating atmospheric effect of oceanic anomalies involves “Atmospheric Model Intercomparison Program (AMIP) type” experiments. In these simulations, SST anomalies are specified as the lower boundary condition of atmospheric general circulation models (AGCM; e.g., Palmer and Sun 1985; Pitcher et al. 1988; Lau and Nath 1994; Kushnir and Held 1996; Lau and Nath 1996; Blade 1997, etc.).

The results of these simulation runs are diverse and often confusing. In the 500-mb geopotential height (Z500) field, the atmospheric response ranges from weak and inconsistent (e.g., Lau and Nath 1994; Kushnir and Held 1996) to significantly strong (Palmer and Sun 1985; Latif and Barnett 1994). This variation can be attributed to the mix of equivalent barotropic response to the surface SST anomalies with a downstream trough growing with height (Pitcher et al. 1988; Kushnir and Lau 1992), and a purely baroclinic response to the SST anomalies with a surface trough and a downstream upper-level ridge (Peng et al. 1997)

Peng et al. (1997) and Peng and Whitaker (1999) addressed this variation by stressing the nonlinear nature of climate response to the imposed forcing. They argued that the atmospheric response to midlatitude SST anomalies crucially depends on the background flow and the role of the transient eddies in the maintenance of the anomalous circulation. In particular, they found that weaker than normal mean meridional winds downstream of the SST anomalies produce a blocking-type, equivalent barotropic response that is hypothesized in the Latif–Barnett (1994, 1996) coupling mechanism. However, this explanation is not applicable on timescales greater than a month due to intrinsic drawbacks of AMIP experiments.

Saravanan and Chang (1999) argued that the main inherent disadvantage of “AMIP-type” simulations of

low-frequency climate variability lies in the postulate that SST anomalies accurately describe boundary forcing on the atmosphere, which, effectively, translates into the assumption that the heat capacity of oceanic mixed layer is infinitely large. In fact, large oceanic mixed layer heat capacity, and therefore strong damping implied by prescribing SST can lead to a systematic response of ensemble atmospheric model integrations forced by anomalies of SST (Rodwell et al. 1999; Mehta et al. 2000). However, this response may neither indicate the atmospheric state that generated SST anomalies in the first place, nor imply active coupling from the ocean to the atmosphere (e.g., Bretherton and Battisti 2000).

The assumption of the infinitely large oceanic mixed layer heat capacity does not hold on timescales longer than a month characteristic of the SST response to the atmospheric forcing. Therefore, low-frequency SST anomalies are driven by air–sea heat fluxes due to internal atmospheric variability, air–sea feedbacks (Frankignoul and Hasselmann 1977; Barsugli and Battisti 1998; Blade 1997; Bhatt et al. 1998), and the dynamics of the mixed layer. The dynamical perturbations are caused by local atmospheric forcing, and by oceanically induced variations of the surface layer heat budget that are independent of the current state of the atmosphere. The latter include changes of oceanic advection, thermocline depth, or temperature of waters entering the mixed layer, and result from past climate variations. These changes represent the “memory” of low-frequency climate variations and therefore the predictable aspect of decadal climate variability (e.g., Latif and Barnett 1994). Therefore anomalies of the mixed layer heat budget, rather than anomalies of surface temperature (which are then a part of the response in the upper-ocean–atmosphere system) need to be prescribed for determining the role of air–sea feedback in decadal climate variations.

In this paper, we investigated the response of a coupled atmosphere mixed layer ocean model to prescribed perturbations of the oceanic heat budget. In particular, we focus on the North Pacific since, as was mentioned before, the possible forecast of climate variations over North America requires an understanding of the physical mechanism underlying changes in this region. While over large areas in the central and eastern North Pacific low-frequency variability in SST results primarily from local atmospheric fluxes (Barnett et al. 1999; Pierce et al. 2001), in the western boundary region (i.e., Kuroshio Current extension region) oceanic perturbations indicative of past, basinwide atmospheric forcing, significantly influence SST (Xie et al. 2000; Miller and Schneider 2000). Therefore, we will concentrate on investigation of the atmospheric response to the perturbation of the surface layer heat budget in this region.

The main questions to be investigated are as follows:

- Can we detect a systematic statistically significant atmospheric response to this forcing?

- If so, what is the physical mechanism of the atmospheric response to the imposed perturbations of the upper-ocean heat budget?
- Are the changes of air–sea fluxes of heat and momentum consistent with hypothesized dynamics of decadal variability (e.g., Latif and Barnett 1994, 1996)?

Another important question concerning low-frequency variability in midlatitudes is to what degree it is teleconnected from the Tropics. As was mentioned by Pierce et al. (2001) the answer to this question has a significant implication to the prediction scheme. If the Tropics play a crucial role in inducing low-frequency variability in midlatitude North Pacific, then the modeling efforts should be aimed toward prediction of the tropical Pacific, and toward understanding of the nature of the teleconnection. On the other hand, if the most part of the North Pacific low-frequency variability is independent of the Tropics, than local midlatitude dynamics should be predicted instead. We address this question by simulating the atmospheric response to the oceanic heat fluxes perturbations located in the central tropical Pacific and comparing it to the response to local forcing. Again, we investigated the significance of the midlatitude response in the light of internal variability of the atmosphere, the physical mechanism of the atmospheric response, and patterns of the changes of air–sea fluxes of heat and momentum.

The manuscript is organized as follows. Section 2 presents a description of the model and the experiment design. In section 3 we will discuss the results of a sensitivity experiment to mixed layer heat budget perturbations located in the tropical Pacific, in an area where a vigorous ocean to atmosphere feedback exists. Section 4 analyzes the atmospheric response to perturbation in the Kuroshio–Oyashio extension (KOE) region, followed in section 5 by a description of the dynamics of the response via atmospheric vorticity and heat budgets. Section 6 discusses the atmospheric response in light of hypothesis for decadal variations.

2. The model and experimental design

a. Model description

The simulations were conducted with the National Center for Atmospheric Research (NCAR) Community Climate Model (CCM3; see Hurrell et al. 1998) coupled with the Slab Ocean Model (SOM). CCM3 is a global spectral (in horizontal direction) model with T42 spectral resolution (approximately $2.8^\circ \times 2.8^\circ$). There are 18 vertical levels in a generalized terrain-following hybrid vertical coordinate. A detailed description of physical parameterization can be found in Kiehl et al. (1998).

The SOM consists of a single prognostic equation for oceanic mixed layer temperature T_0 :

$$\rho_0 C_0 h_0 \frac{\partial T_0}{\partial t} = F + Q,$$

where Q is ocean mixed layer heat flux simulating deep-water heat exchange and ocean transport, δ_0 is the density of ocean water, C_0 is heat capacity of the ocean water, h_0 is monthly varying ocean mixed layer depth specified from the Levitus (1982) climatological annual cycle, and F is net atmosphere to ocean heat flux. In the absence of the ice, F is defined as the sum of solar flux absorbed by the ocean (FS), long-wave cooling flux (FL), sensible heat flux from the ocean into the atmosphere (SH), and latent heat flux from ocean to atmosphere (LH):

$$F = FS - FL - SH - LH.$$

In the presence of the sea ice, the mixed layer temperature tendency vanishes, and an additional mixed layer depth tendency term due to the heat of fusion of sea ice emerges. For more detailed description of SOM, readers are referred to Kiehl et al. (1998).

The monthly values of Q are tuned (by a long control run of a coupled model) in such a way that the simulated annual cycle of SST is realistic. Typical values for Q are from 0 to 150 W m^{-2} in the winter hemisphere, and 0 to -150 W m^{-2} in the summer hemisphere. The sign convention is as follows: positive values of Q mean that heat is transferred from the ocean into the atmosphere. It is this term that is augmented by a prescribed, regional perturbation in the experiments described here.

b. Control run

To examine the model applicability to studying the midlatitude atmosphere–ocean coupling, mean state and internal variability of 65 yr of the control simulation were validated against the observations. The control run was performed by integrating the coupled model forced with climatological seasonal cycle of ocean mixed layer heat flux Q , and ocean mixed layer depth h . Our focus was on the near-surface variables (wind stress, associated with it Sverdrup transport, air–sea heat flux, SST) and also on midtropospheric circulation measured by anomalies of Z500. If not stated otherwise, we will discuss the wintertime [averaged over Dec–Feb (DJF)] response.

The observed wintertime low-frequency variability of Z500 as well as sea level pressure (SLP) fields manifest two robust modes over the North Pacific: 1) the Pacific–North American (PNA) pattern and 2) the western Pacific (WP) pattern (Wallace and Gutzler 1981). These two modes explain more than 50% of internal variability of the atmospheric circulation and therefore a good model skill in reproducing these two harmonics is significant for accurate simulation of the ocean–atmosphere coupling in midlatitudes.

A principal component analysis of the monthly mean Z500 anomalies revealed that the first empirical orthogonal function (EOF), shown in Fig. 1a, corresponds to the familiar WP pattern with a dominant ridge/trough occurring near (45°N , 170°W) and opposite sign anom-

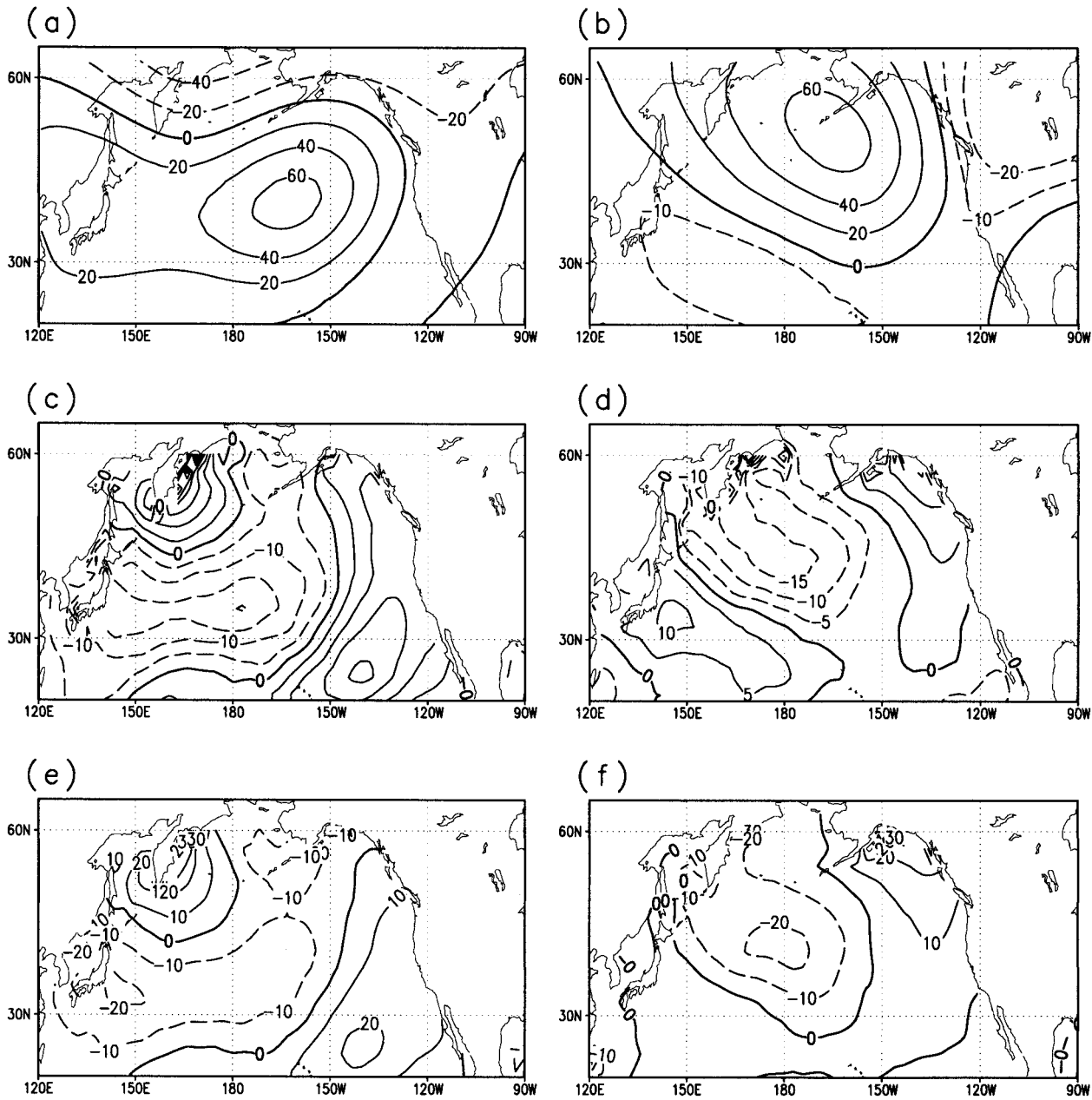


FIG. 1. (a) First and (b) second EOF of Z500 of the 65 winters (DJF) of the control run, contour interval 20 m. Regression of the sum of latent and sensible heat fluxes onto (c) 1PC and (d) 2PC of Z500 of the control run, contour interval 5 W m^{-2} . (e) First and (f) second EOF of sum of latent and sensible heat flux of the 65 winters (DJF) of the control run, contour interval 10 W m^{-2} . Negative values are dashed.

alies (trough/ridge) occurring over western Canada. This mode explains 33% of the variance compared to 20% explained by the second EOF. The second EOF (Fig. 1b) bears resemblance with the PNA pattern discussed in Wallace and Gutzler (1981) but is shifted southeastward. The spatial structure of this pattern exhibits a ridge with a local maximum at around (55°N , 170°W), and a trough over the continent. Thus in the control run the WP pattern is slightly dominant, which is similar to

the AMIP-type experiment with a climatological annual cycle of monthly mean global SST and sea-ice distribution where a WP-like pattern explains a larger part of the variance (e.g., Saravanan 1998). Comparison with observations indicated that the leading two EOFs of Z500 (Figs. 2a–b) obtained from 1949–2000 National Centers for Environmental Prediction (NCEP)–NCAR reanalysis (Kalnay et al. 1996) are very similar but of opposite order to those of the unforced model. Except

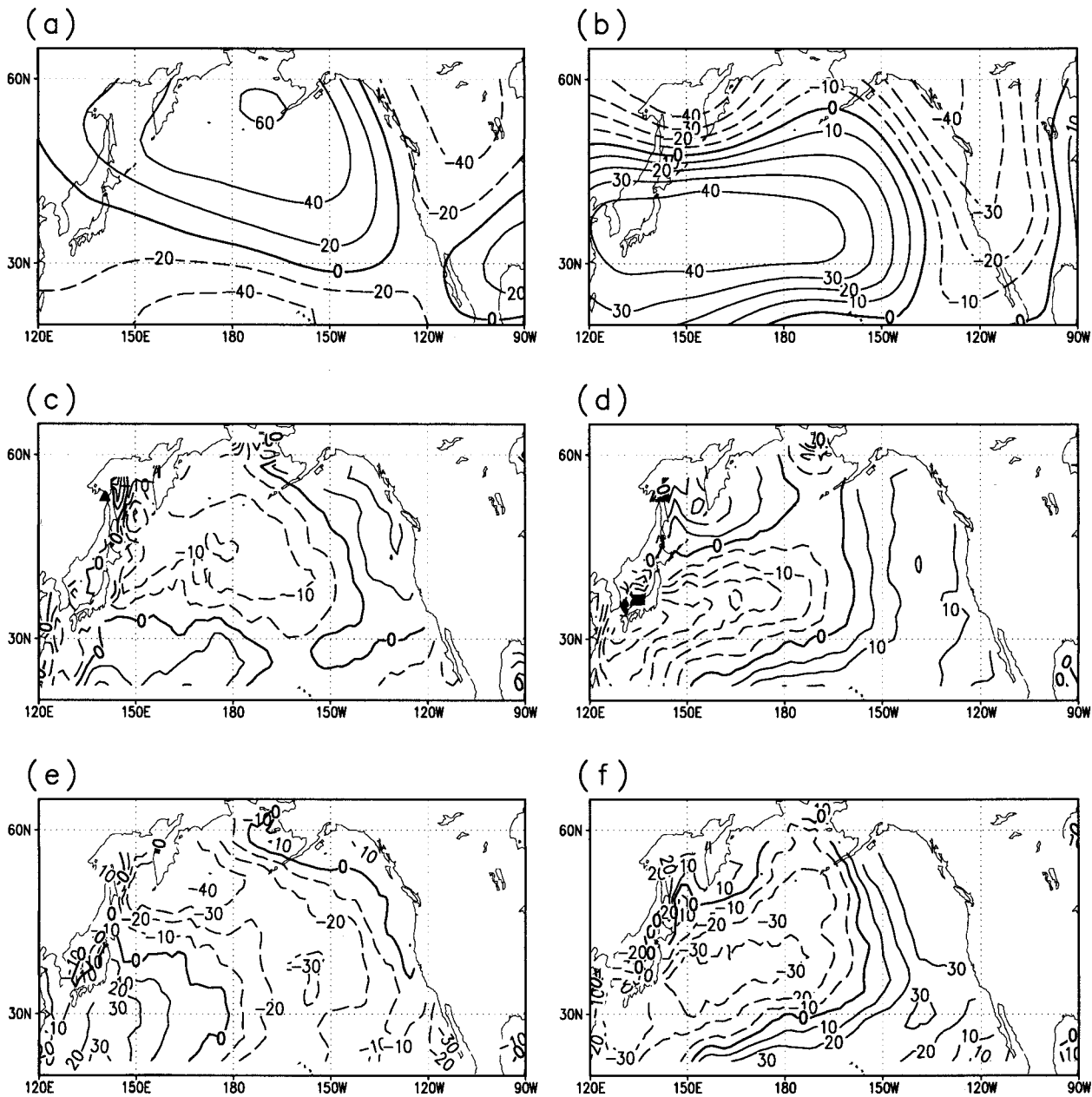


FIG. 2. Same as Fig. 1 but for NCEP–NCAR reanalysis 1949–99 data. Note that EOFs are of opposite order to those shown in Fig. 1.

for some minor discrepancies, the first EOF explaining 29% of total variance (Fig. 2a) very well matches the second EOF of the control run (Fig. 1a) while the second EOF explaining 23% of total variance (Fig. 2b) resembles the first EOF of the control run (Fig. 1b). The dominance of the WP pattern in the simulations forced with a climatological seasonal cycle of ocean mixed layer heat flux (or SST) can be explained by the fact that WP pattern counterpart at SLP is strongly coherent with climatological mean SLP (see Wallace et al. 1990).

Atmospheric low-frequency variability drives (at least in part) large-scale low-frequency anomalies of the

surface heat fluxes (e.g., Saravanan 1998). Therefore the credibility of the model also depends on the skill of reproducing spatial correlation between surface heat fluxes and the leading modes of Z500. The anomalies of turbulent air–sea heat fluxes (the sum of sensible and latent heat components) associated with the two modes of Z500 internal variability were determined by regression onto the normalized leading principal components (PCs) of Z500.

Though there are some discrepancies in the amplitude and geographic location, the spatial structure of the simulated turbulent heat fluxes associated with WP mode

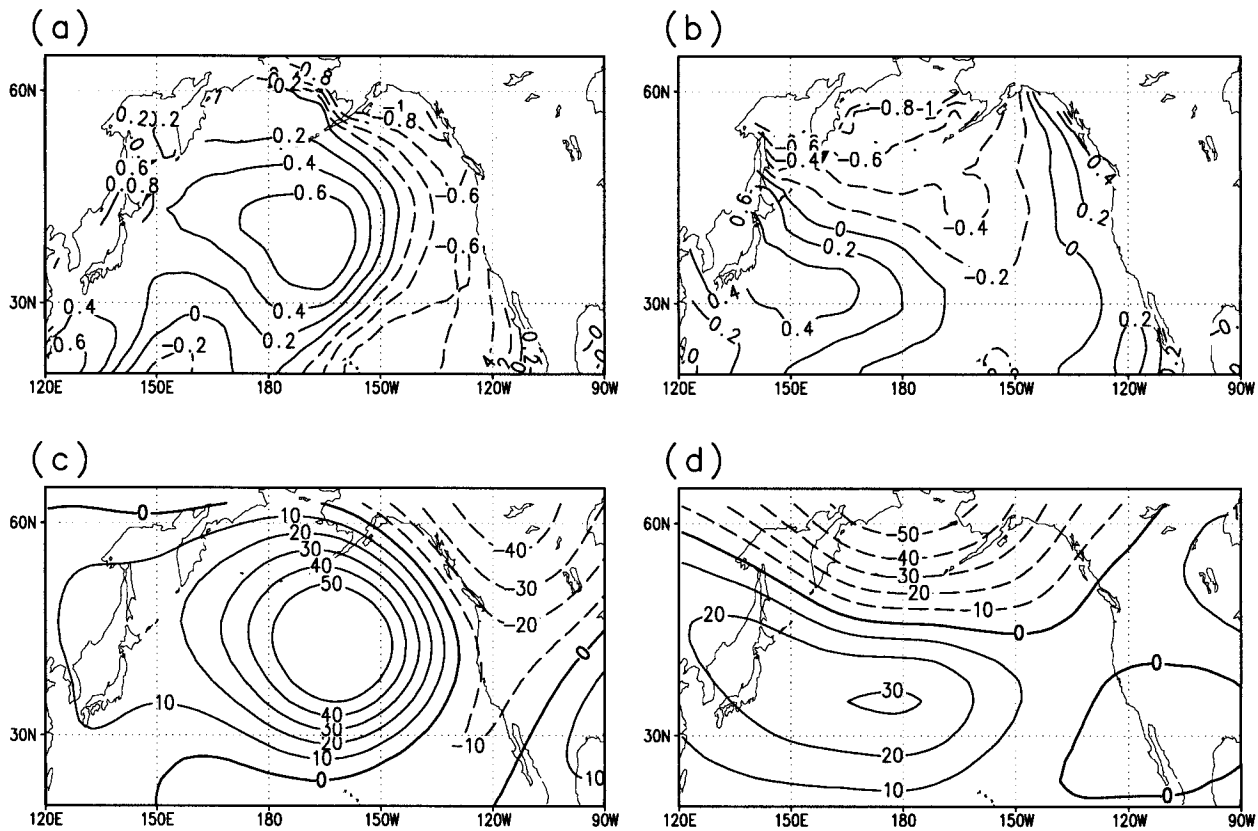


FIG. 3. (a) First EOF of the wintertime SST of the control run, contour interval 0.2 K, negative values are dashed; (b) second EOF of the wintertime SST of the control run, contour interval 0.2 K, negative values are dashed; (c) regression of the Z500 of the control run onto 1PC of the wintertime SST anomalies of the control run, contour interval 10 m, negative values are dashed; (d) regression of the Z500 of the control run onto 2PC of the wintertime SST anomalies of the control run, contour interval 10 m, negative values are dashed.

(Fig. 1c) is similar to the observations (Fig. 2d). The pattern correlation coefficient of the model heat fluxes regression map with the first EOF of the latent and sensible heat flux anomalies (shown in Fig. 1e) is 0.96 which is statistically significant at 99% significance level. The corresponding correlation coefficient for the reanalysis data is 0.87. In comparison to the observations (Fig. 2c), the spatial structure of the simulated turbulent heat fluxes associated with the PNA mode of variability (Fig. 1d) is shifted northwestward. The correlation between this mode and the second EOF of the latent and sensible heat flux anomalies (shown in Fig. 1f) is 0.89. The corresponding observational modes are shown in Figs. 2c and 2e. Observed first mode of low-frequency surface heat flux variability (Fig. 2e) is less coherent with the atmospheric circulation (Fig. 2c) than simulated variability. This discrepancy can be explained by the absence of the Ekman advection in our model. Thus the changes in the heat flux at the surface in the model are completely defined by the atmosphere. The statistics depicted above agrees with the findings of Cayan (1992) and Alexander and Scott (1997) stating that in the North Pacific the connection between the atmospheric circulation and surface latent and sensible heat flux anomalies

is not local, but rather basin-scale and is associated with the main modes of atmospheric variability.

The analysis of the spatial pattern of the first (explaining 24% of the total variance) and second (explaining 16% of the total variance) empirical modes of the SST field of the unforced run shown in Figs. 3a and 3b reveals fair resemblance with the corresponding modes of the observed SST field from the Global Sea-Ice and SST version 2 (GISST) dataset (see Fig. 9 in Saravanan 1998).

The regression of Z500 onto the first PC of the SST (Fig. 3c) resembles the WP pattern (shown in Fig. 1a) with the pattern correlation of 0.72 that is 95% significant. The regression of Z500 onto the second PC of the SST (Fig. 3d) resembles the PNA-like pattern (Fig. 1b) shifted northwestward ($r = 0.56$). It should be noted that these simultaneous regression patterns do not allow drawing any cause-and-effect conclusion on the physical mechanism of the ocean-atmosphere interaction in mid-latitudes.

Theoretical changes in the ocean circulation may be calculated from the simulated surface wind stress patterns. One of the simplest theories of the steady-state response of the large-scale oceanic circulation in the

North Pacific to the atmospheric wind stress can be described by the Sverdrup relation that postulates the balance between wind stress curl and meridional advection of planetary vorticity by the oceanic circulation. Thus, the correct spatial distribution of the simulated surface wind stress pattern in the North Pacific is crucial for atmosphere–ocean coupling in midlatitudes. The mean wind stress (Fig. 4a) compares favorably with the mean obtained from the NCEP–NCAR 1961–91 reanalysis data (see Fig. 4a in Deser et al. 1999). Westerly wind stress anomalies cover much of the basin with maximum values at around 45°N. The corresponding wind stress curl is positive north of 45°N and negative south of 45°N as in observations. Integrating the curl field westward from the coast of North America yields the Sverdrup transport ψ defined as

$$\psi(x) = -\frac{f}{\beta\rho} \int_{x_E}^x \mathbf{k} \cdot \left(\nabla \times \frac{\boldsymbol{\tau}}{f} \right) dx',$$

where f is a Coriolis parameter, β is its meridional derivative, $\boldsymbol{\tau}$ is the wind stress, ρ is the density of the ocean water, and X is the longitude. Here X_E represents the longitude of the eastern boundary of the ocean; \mathbf{k} signifies a unit vector in the vertical direction.

Sverdrup transport (Fig. 4b) shows a familiar pattern of anticyclonic flow in the subtropical gyre, and cyclonic flow of the subpolar gyre. Both strength and spatial pattern of the simulated Sverdrup transport resemble Sverdrup transport calculated using wind stress from NCEP reanalysis data for 1968–91 (see Fig. 5a in Deser et al. 1999).

In summary, the coupled model produces realistic patterns and a relationship between the surface variables and midtropospheric flow, so that we can have some faith in the relevance of the experimental results presented in this paper.

c. Experimental design

As mentioned in the introduction, the main goal of our study is the investigation of midlatitude response of the coupled atmosphere mixed layer ocean model to prescribed disturbances of the mixed layer heat budget that mimic low-frequency oceanic perturbations of the surface heat budget.

Some recent studies (Deser et al. 1999; Miller et al. 1994; Xie et al. 2000) suggest that there are two complementary modes of decadal variability in the North Pacific. One is teleconnected from the Tropics, and another is associated with the KOE. To test this idea we prescribed forcing in geographic regions where oceanic perturbations are known to actively affect the surface heat budget. These potentially predictable surface regions were determined by conducting a hindcast experiment with a stand-alone oceanic GCM. Hamburg Ocean Primitive Equation model was forced with observed 1965–2000 NCEP–NCAR surface wind stress

anomalies (for detailed description of the model see Pierce 1996). The simulated SST anomalies reveal two main regions of low-frequency variability produced by large-scale ocean dynamics. The first region is located in the KOE while the second area is located in the central tropical Pacific. Therefore, two sets of experiments were performed. In the first set the model was forced with a constant in time anomalous oceanic heat flux Q located in the central tropical Pacific as shown in Fig. 5a. The second set of experiments involved the investigation of the global response to forcing localized in the North Pacific, in the region of the KOE (Fig. 5b). In both cases the model was run for 10 yr with positive oceanic heating and for 10 yr with negative oceanic heating. The wintertime response was defined as the difference (response to positive ΔQ minus response to negative ΔQ) between the simulated monthly mean values of SST, geopotential height, SLP, surface wind stress, precipitation, energy fluxes at the surface, etc., averaged over DJF. Thus, if not specified differently, the magnitude of oceanic forcing is considered to be $2 \times \Delta Q$. The statistical significance of the response was evaluated using Student's t-test (Spiegel 1991). Each of the 10 winter runs within the ensemble was treated as independent, therefore, individual ensemble possesses 9 effective degrees of freedom. Furthermore, signal-to-noise ratio (defined as absolute value of the mean response divided by the standard deviation of the DJF mean values of the control run) was analyzed. This ratio can be viewed as a measure of model sensitivity to a prescribed forcing. Though the imposed mixed ocean layer heat flux perturbations in our experiments were set to be constant in time they should be thought of as varying with timescales much longer than the typical atmospheric adjustment timescale.

3. Tropical forcing

To investigate the role of the Tropics in producing low-frequency variability in the midlatitude North Pacific we studied the response of our coupled model to the mixed layer heat flux disturbances prescribed in the tropical Pacific. In the region shown in Fig. 5a the oceanic mixed layer heat flux was perturbed with a stationary bell-shaped function with a maximum of 20 W m⁻² at the equator and 150°E. When integrated over the forcing region, it corresponds to approximately 10% of the amplitude of the annual cycle.

Response to perturbations of the oceanic heat flux described above is displayed in Fig. 6. Shading indicates the regions where response is more than 95% significant. As seen in Fig. 6a, the positive mixed layer heat flux anomaly leads to significant changes of SST in the region of the forcing, south to the location of the forcing, in the region of subpolar gyre, and in the central North Pacific. The changes in the SST pattern correspond to anomalous wind stress shown in Fig. 6c. The flow is convergent over the warm SST anomalies at the equator.

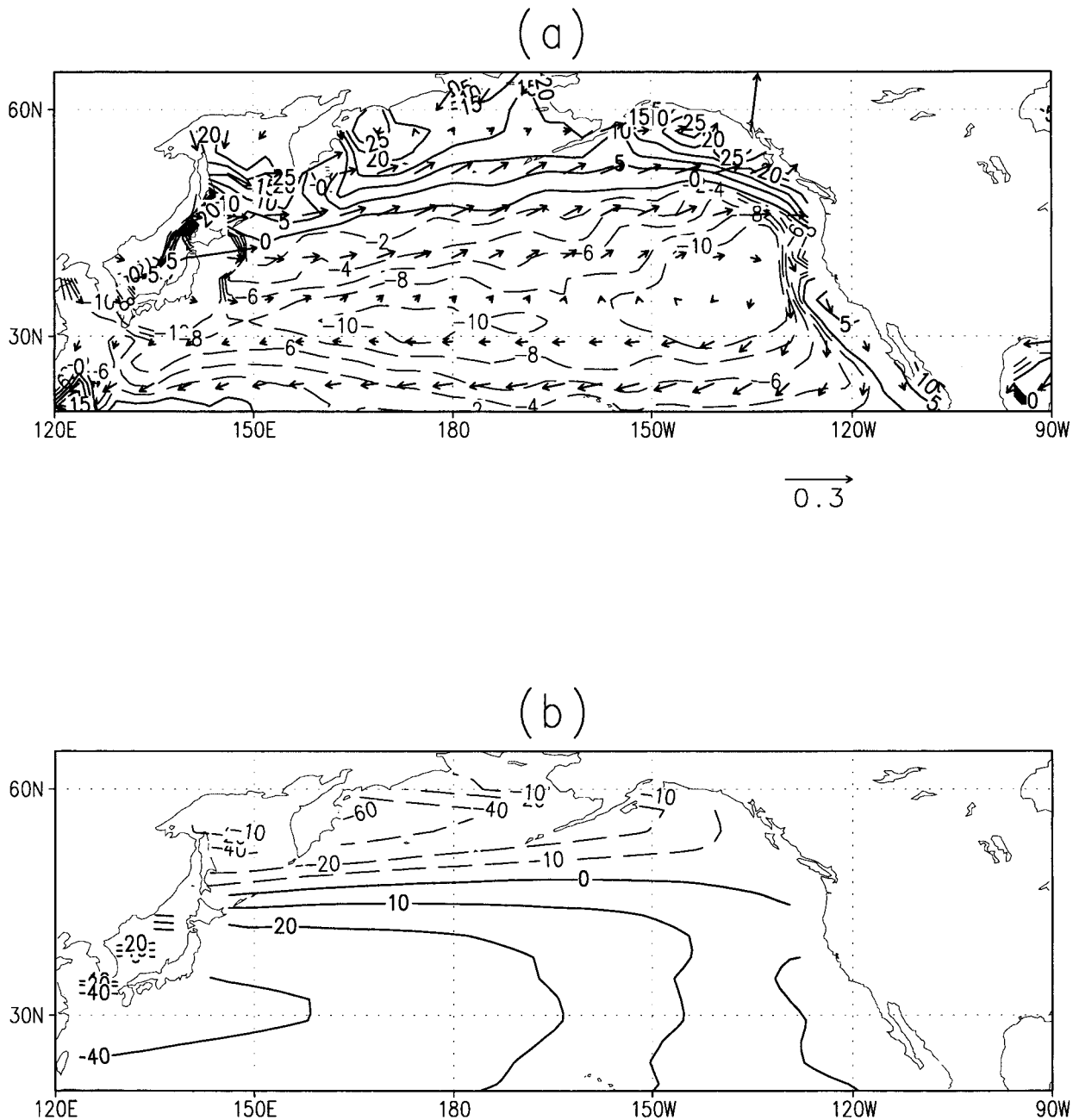


FIG. 4. The 65-yr average of the control run: (a) surface wind stress (vectors, N m^{-2}) and its curl, (contours, interval $2 \times 10^{-8} \text{ N m}^{-3}$ for negative contours and $5 \times 10^{-8} \text{ N m}^{-3}$ for positive); (b) corresponding Sverdrup streamfunction, contour interval 20 Sv ($1 \text{ Sv} \equiv 10^9 \text{ kg s}^{-1}$), contour 10 Sv is also included. Negative values are dashed.

The changes in the surface wind pattern lead to the changes in atmosphere to ocean heat fluxes (Fig. 6e) and the prescribed heat flux perturbation in the central tropical Pacific is balanced locally by latent heat flux and incoming solar radiation perturbations. In response to the oceanic heating, the centers of deep convection (manifested in the precipitation pattern, shown in Fig. 6f) intensify and shift, therefore exciting global atmospheric response by modulating the Hadley circulation

and corresponding indirect circulation in the subtropics and midlatitudes. The global response includes significant anomalies of 500-mb geopotential height (Fig. 6d) with centers of action over the North Pacific and North America that resemble the PNA pattern of internal variability (e.g., Wallace and Gutzler 1981; Kushnir and Wallace 1989). Comparison of SLP pattern (Fig. 6b) and Z500 field (Fig. 6d) reveals similar structures of these two fields (pattern correlation coefficient ~ 0.8).

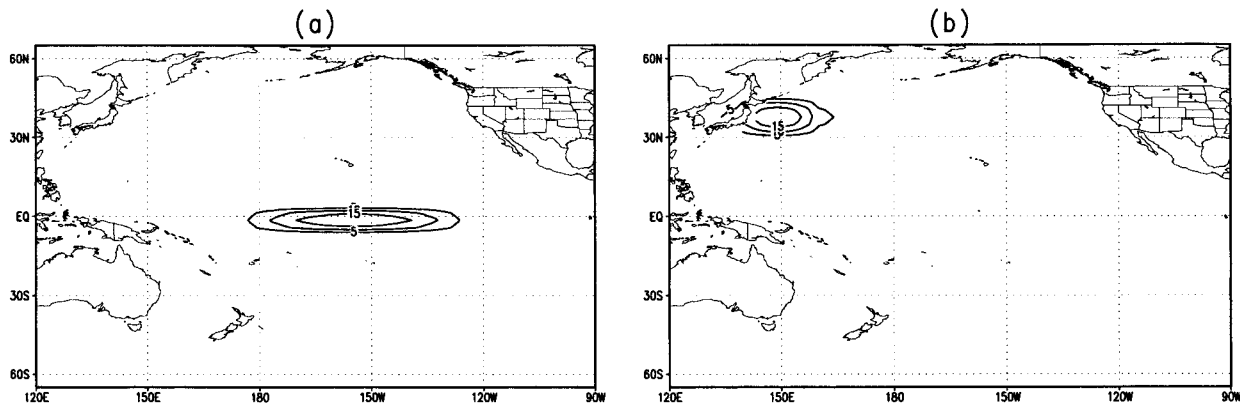


FIG. 5. Prescribed mixed layer ocean heat perturbations (a) in the central tropical Pacific and (b) in the Kuroshio extension region, contour interval 5 W m^{-2} .

The changes of the surface pressure field over the North Pacific lead to reorganization of the surface winds over the basin (Fig. 6c) and, thus, of the turbulent air–sea heat fluxes that crucially depend upon the surface winds. To balance this, SST is modified in a way that leads to compensation of the air–sea difference. The SST response is tilted southeastward with an extremum of -1.5 K west of the Aleutian low region. Mean SST change over the Kuroshio extension region is close to -0.3 K , which is comparable with the standard deviation of the SST anomalies in this region. In the North Pacific basin the structure of SST anomalies resembles the second mode of the internal SST variability of the control run with a pattern correlation of 0.7 (90% significance level). This SST pattern corresponds to heat flux anomalies (Fig. 6e) resembling the second mode of heat flux variability of the control run (Fig. 1f). Thus, adjustments in surface variables are associated with the changes in a PNA pattern of the atmospheric circulation.

In summary, the prescription of strong oceanic heat flux forcing in the Tropics is efficient in exciting atmospheric response in both the Tropics and midlatitudes. Heating anomalies of 40 W m^{-2} (positive minus negative anomalies) induce SST anomalies with the maximum amplitude of 1.5 K in the region of the tropical Pacific. The atmospheric response in midlatitudes bears close resemblance with the second (PNA) mode of variability of the unforced run. The corresponding response in SST field in the North Pacific is significantly correlated with the second mode of intrinsic variability of the control run. It is 1.5 times stronger than the intrinsic variability of the unforced run indicating that a part of midlatitude response may be teleconnected from the Tropics. Similar results were obtained in some previous studies on the influence of midlatitude atmosphere–ocean coupling on the midlatitude response to the tropical forcing (e.g., Alexander 1992). It should be noted that tropical forcing causes changes mainly over the central North Pacific. Though, this signal can be transported by oceanic processes to the coast of Japan,

the question remains on the role of the midlatitude heat flux variations in maintaining the low-frequency climate variability over the North Pacific.

4. Midlatitude forcing

As mentioned in the introduction, a crucial question of our study is the degree to which the low-frequency climate variability in the North Pacific arises from the ocean–atmosphere coupling over this region. If the coupling is significant, the deterministic part of low-frequency midlatitude variability must be related to the oceanic processes. Thus, prescription of midlatitude oceanic mixed layer heat disturbances constitutes a physically consistent approach to the specification of the boundary forcing for AGCMs.

In our midlatitude experiment Q was perturbed with a stationary bell-shaped function with a maximum of 20 W m^{-2} at 35°N and 150°E . When integrated over the Kuroshio Current extension region, it corresponds to approximately 5% of the amplitude of the annual cycle in this region. Again, we conducted the integration both for positive and negative perturbations of Q . The choice of the region was dictated by the results of the hindcast experiment described in section 2c. In addition, the findings of Pierce et al. (2001) revealed that ocean dynamics dramatically enhanced decadal timescale SST variability in the Sub Arctic Front Zone–Kuroshio extension region and that this enhancement came from coupled ocean–atmosphere interaction rather than from the ocean dynamics alone.

The simulated response to the prescribed oceanic mixed layer heat anomalies is shown in Fig. 7. The regions with more than 95% significant values are shaded.

Spatial distribution of SST response (Fig. 7a) exhibits warm anomalies in the Kuroshio Current extension that are accompanied by warm SST anomalies in the most of the Pacific, except for the region centered at the date line and 37°N . The signal-to-noise ratio in the Kuroshio

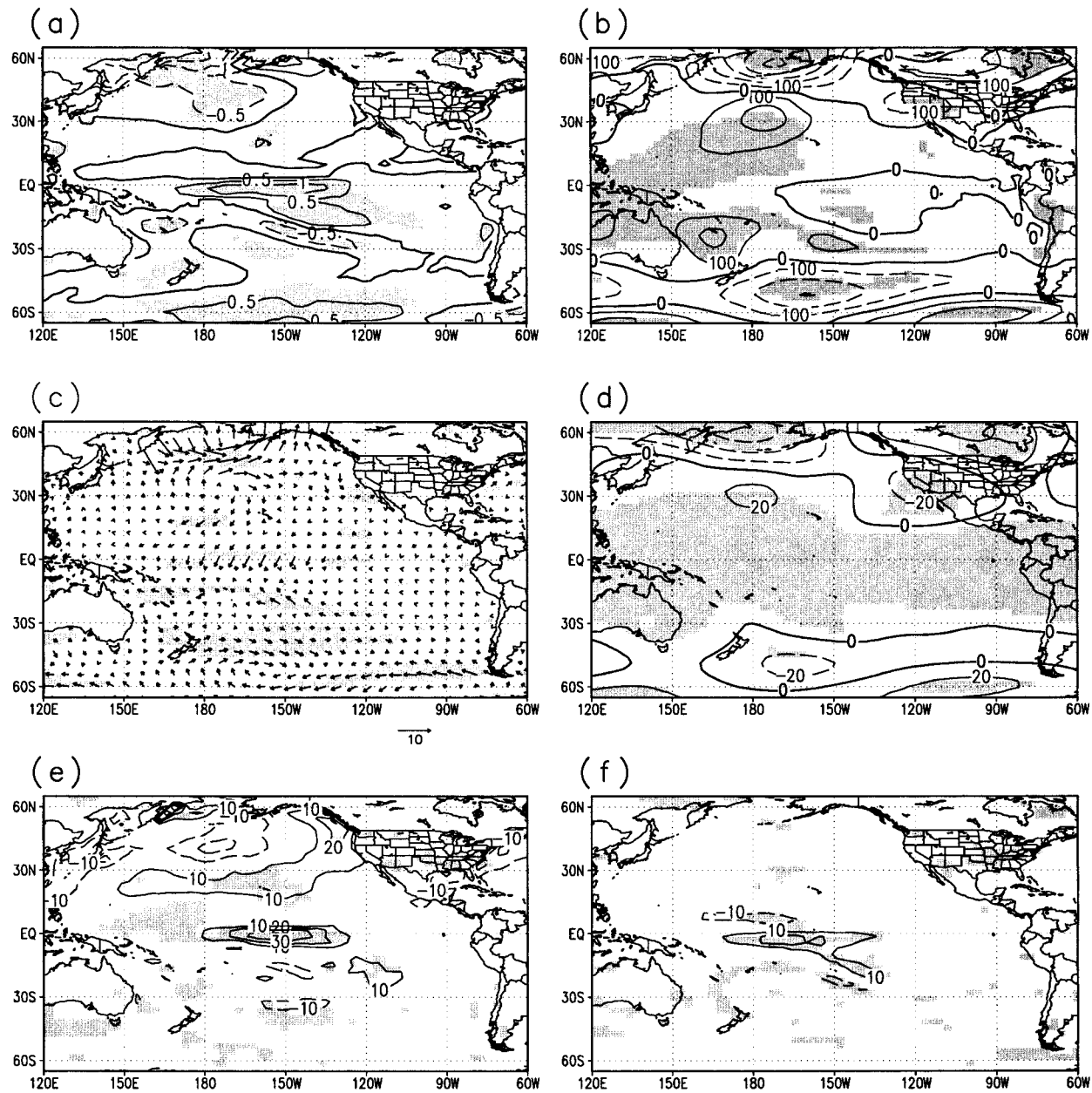


FIG. 6. Wintertime response to the tropical central Pacific forcing shown in Fig. 5a: (a) SST anomalies, contour interval 0.5 K; (b) SLP anomalies, contour interval 100 Pa; (c) vectors, surface wind stress ($1 \times 10^{-2} \text{ N m}^{-2}$); (d) Z500, contour interval 20 m; (e) surface heat flux, contour interval 10 W m^{-2} ; (f) precipitation, contour interval 10 mm month^{-1} . Negative values are dashed. Shading indicates the regions where response is more than 95% significant.

extension region is 3, indicating that a 10% change of the mean oceanic heat fluxes in this region causes SST anomalies larger than 3 standard deviation of the control run. The pattern correlation between this response (with the forcing region excluded) and the second EOF of SST anomalies (SSTAs) of the control run (Fig. 3b) is 0.5 (that is statistically significant at the 90% confidence level in the Monte Carlo experiment).

Since there is no ocean dynamics in the model, the only stabilizing mechanism that is possible consists of

excitation of the atmospheric heat fluxes that damp original SSTAs and balance the prescribed oceanic forcing. The corresponding surface ocean to atmosphere heat fluxes (Fig. 7e) in the KOE region are positive in the region of the positive SSTAs. Surface heat flux anomalies (Fig. 8) are formed mainly by latent and sensible heat flux anomalies (Figs. 8a,b). The changes in the latent heat flux are explained primarily by changes in the relative humidity of the air. Consequently, the increase in SST is balanced locally by changes in the

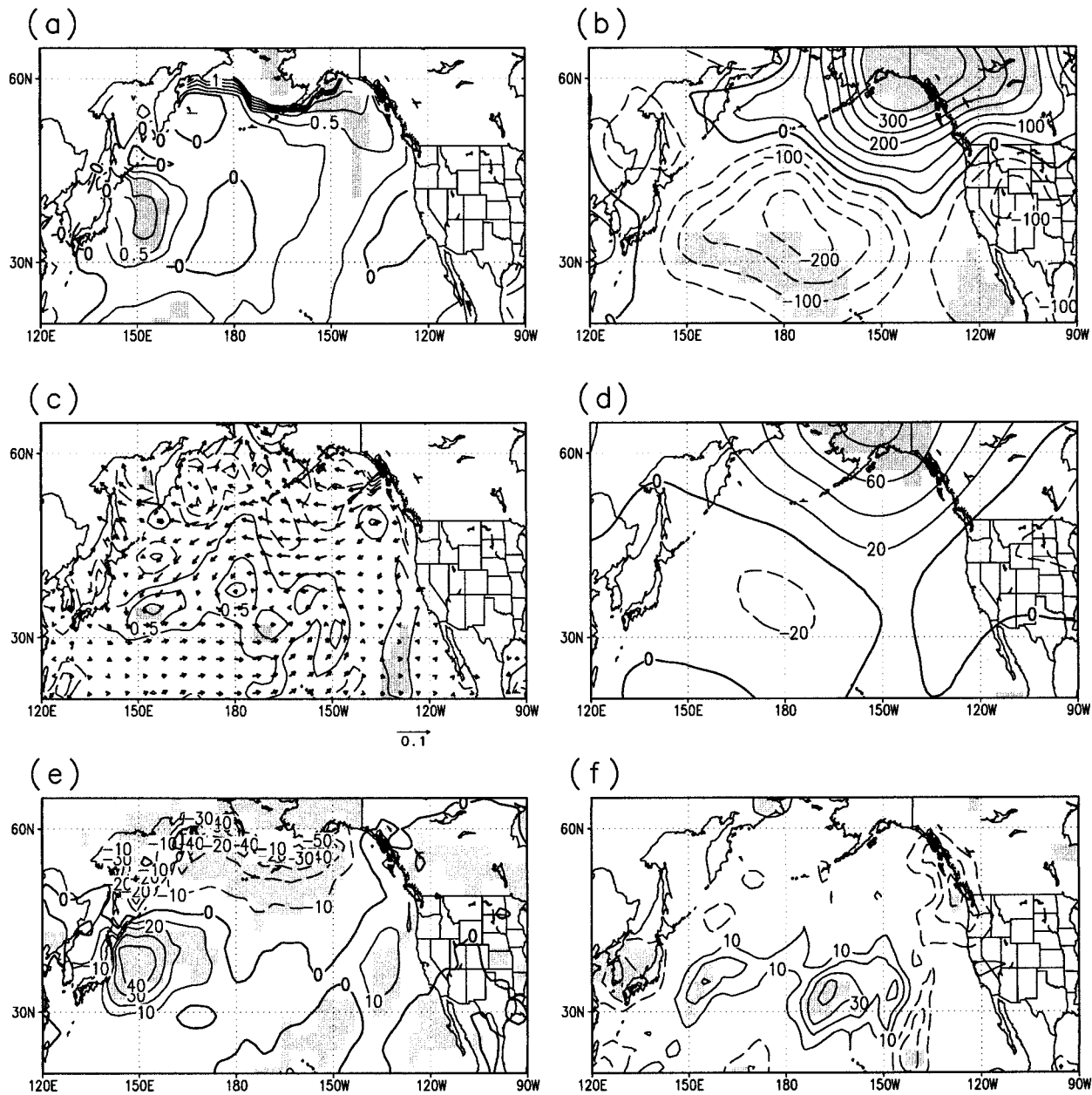


FIG. 7. Wintertime response to the forcing in the Kuroshio Current extension region shown in Fig. 5b: (a) SST anomalies, contour interval 0.25 K; (b) SLP, contour interval 100 Pa; (c) vectors, surface wind stress ($1 \times 10^{-2} \text{ N m}^{-2}$) and Ekman pumping velocity (contours), interval 0.25 m s^{-1} ; (d) Z500, contour interval 20 m; (e) surface heat flux, contour interval 10 W m^{-2} ; (f) precipitation, contour interval 10 mm month^{-1} . Negative values are dashed. Shading indicates the regions where response is more than 95% significant.

saturated humidity rather than by a large-scale rearrangement of the atmospheric momentum expected from the changes of the wind field.

It should be noted that in the subpolar gyre region the sensible (Fig. 8b) heat fluxes play the dominant role during the cold season. The fluxes are negative indicating atmosphere to ocean energy transfer.

Over the midlatitude Pacific, the change in the humidity distribution modifies the spatial structure of the convective heating imposed onto the atmosphere. The

anomalies of the convective heating at different levels are presented as the sequence of the horizontal cross sections of the temperature tendency due to convection. The oceanic heating induces enhanced convection over the heating region. The cross sections of temperature tendencies due to the convection (Fig. 9) indicate that the maximum in convective heating over the Kuroshio extension region occurs at 850 mb. The convective heating over this region shifts eastward with height and is accompanied by a statistically significant precipitation

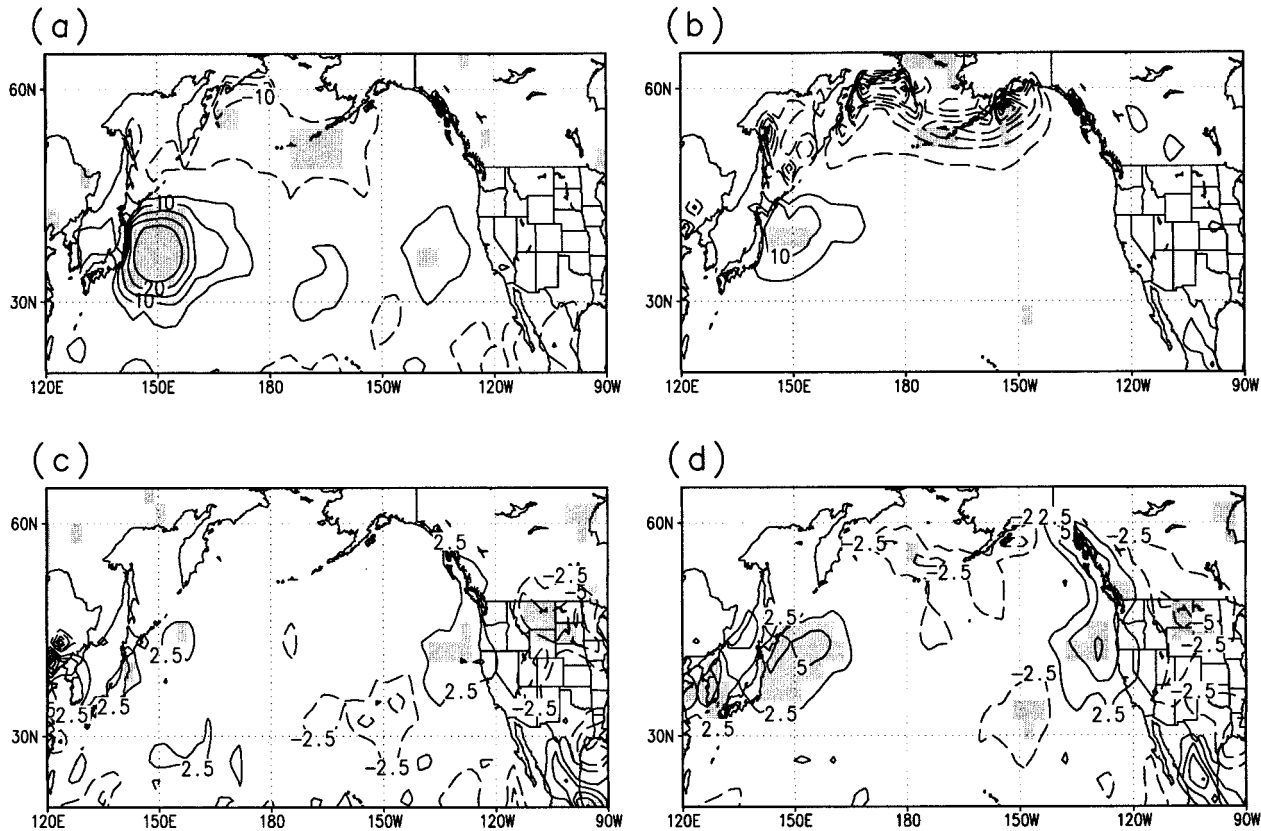


FIG. 8. Wintertime response to the forcing in the Kuroshio Current extension region in the surface ocean to atmosphere heat fluxes, contour interval 5 W m^{-2} . Negative values are dashed. Shading indicates the regions where response is more than 95% significant. (a) Latent heat flux, (b) sensible heat flux, (c) shortwave solar heating, and (d) longwave radiation.

pattern centered at $(35^\circ\text{N}, 155^\circ\text{E})$ shown in Fig. 7f. The second “warming” region is located at $(35^\circ\text{N}, 170^\circ\text{W})$. The amplitude of the convective adjustment heating over this region grows with height and reaches the maximum of 1 K day^{-1} at 500-mb height. The corresponding precipitation anomalies (Fig. 7f) are greater than 40 mm month^{-1} and are 95% significant in this region. Geographic location of this center of action coincides with the extremum of the first leading EOF of the atmospheric surface heat flux anomalies of the control experiment (Fig. 1e). As it was mentioned in section 2b, this mode of surface heat fluxes is coherent with the WP pattern of Z500 variability.

The atmospheric heating anomalies described above induce a dynamical response in the troposphere. There is a statistically significant signal in vertical velocity (Fig. 10) in both regions. Over the KOE region the precipitation pattern exhibits a north–south dipole. This structure suggests a shift in convection activity rather than just an intensification. Walter et al. (2001) argued that this nonlinear behavior is sensitive to the position of the forcing relative to the storm track due to the important role of the transient eddies feedback in maintaining the atmospheric response to midlatitude thermal forcing. The vertical velocity rapidly vanishes with

height over the KOE region. The ascent over the “second center of action” observed at all heights reaches its maximum at around 500 mb. This ascent is accompanied by a downward motion at the west coast of Alaska and the United States, which is associated with less precipitation and less convective heating in this region. The later feature might be of significant importance to the climate variations over the west coast of the continent.

The corresponding northward meridional velocity field (Fig. 11b) weakens west of the date line and east of 150°W . However, the northward velocity strengthens in the latitudinal belt between the date line and 150°W . This reorganization leads to weaker cold-air advection into the region west of the date line, and stronger cold-air advection east of the date line.

The matching height–longitude cross section of the anomalous geopotential height at 40°N (Fig. 12) reveals a trough growing with height downstream of the heating region. To the east of it a geopotential ridge growing with height emerges. At 500 mb, the response in the geopotential height (Fig. 7d) resembles the second EOF (PNA pattern) of the control run shown in Fig. 1b (pattern correlation = 0.52). The manifestation of this pattern at the surface (shown in Fig. 7b) reveals the neg-

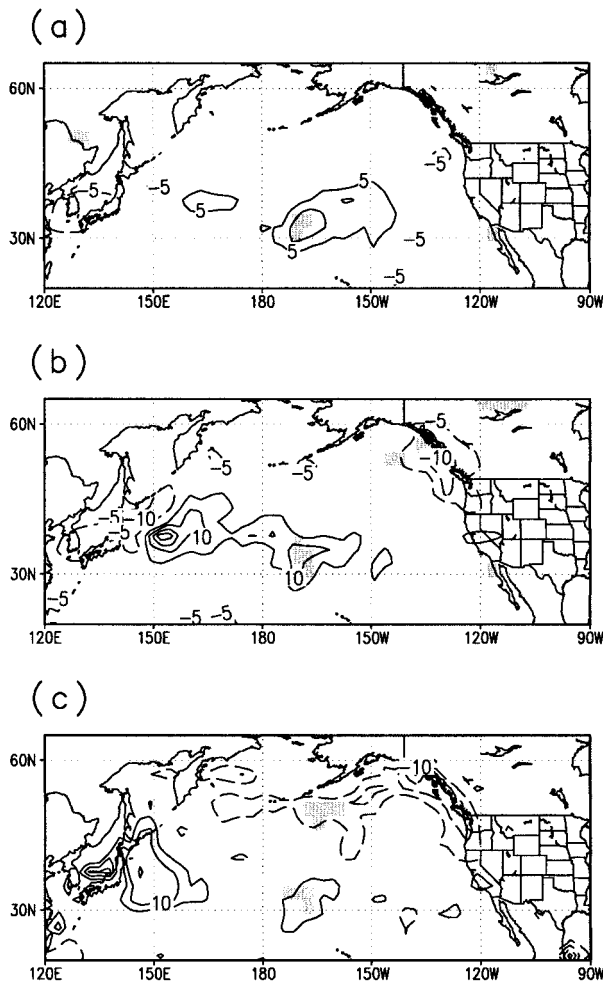


FIG. 9. Wintertime temperature tendencies due to the convective adjustment processes contour interval $5 \times 10^{-6} \text{ K s}^{-1}$. Shading indicates the regions where response is more than 95% significant. (a) 500-mb height, (b) 700-mb height, (c) 850-mb height.

ative SLP anomalies, and thus stronger cyclonic activities over the same “region of action” centered at (37°N , 170°W).

These changes in SLP induce response in the wind stress field shown in Fig. 7c. The zonal wind stress pattern exhibits a north–south dipole structure with the positive anomalies centered at the region of the Pacific subtropical gyre, and negative anomalies centered north of 40°N indicating weakening of westerlies north of the heating region, and weakening of the trade winds south of the heating. The corresponding changes in the Ekman pumping velocity (shown in Fig. 13a) reach their maximum over the region of action located at (37°N , 170°W). The possible reorganization of the oceanic northward Sverdrup transport (Fig. 13b) exhibits weakening in midlatitude western and central Pacific and strengthening in high latitudes. The Sverdrup transport anomalies are 2 times stronger than one standard deviation of the control run. The implicit changes of the

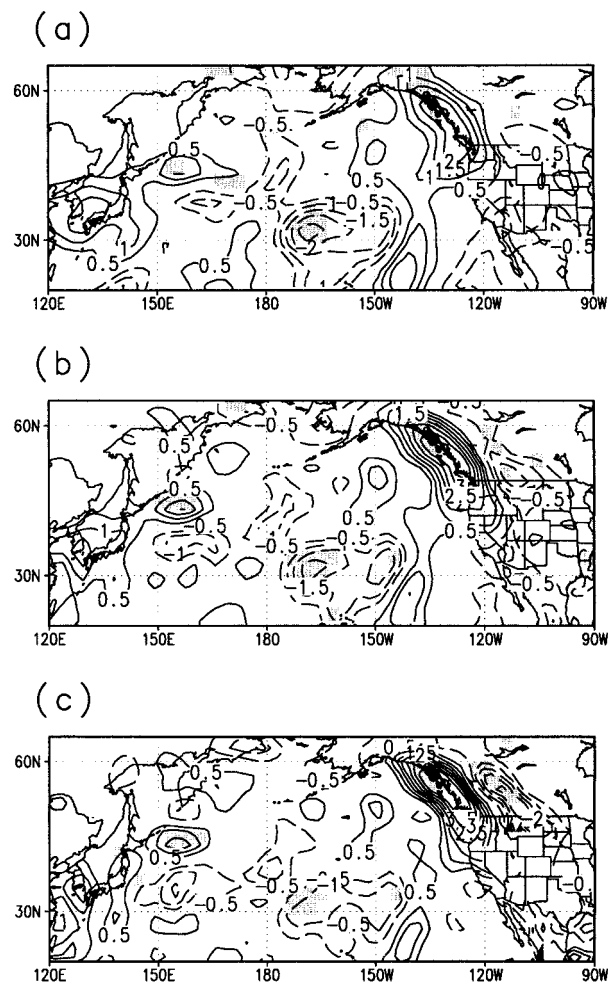


FIG. 10. Wintertime vertical velocity anomalies at different pressure levels, contour interval $0.5 \times 10^{-2} \text{ Pa s}^{-1}$. Shading indicates the regions where response is more than 95% significant. (a) 500-mb height, (b) 700-mb height, (c) 850-mb height.

western boundary currents cool the ocean in the Kuroshio extension region due to the decrease of Kuroshio transport. At the same time the cooling due to Oyashio is also reduced and will cause warm SST anomalies off the coast of Kamchatka. The pattern of the annual mean Sverdrup transport (not shown here) strongly resembles the wintertime response but is twice weaker indicating that the atmosphere forces the ocean mainly during the cold season.

The most interesting feature revealed from these simulations is the existence of nonlocal response in the wind stress field and associated with it a possible change in the oceanic transport. The sign of this reorganization crucially depends on the balance between changes in the Kuroshio and Oyashio regions. These findings indicate that there exists an atmospheric feedback to the boundary forcing that tends to force oceanic dynamics to counteract an original anomalous heating. Thus, there

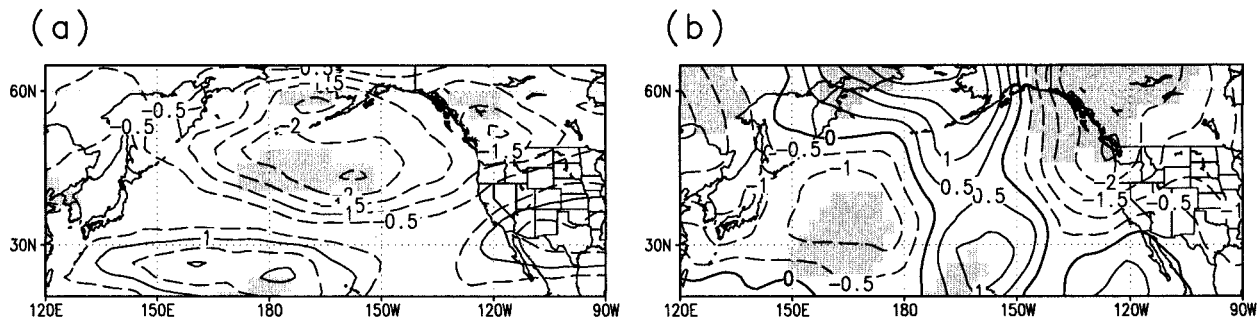


FIG. 11. (a) Zonal wintertime wind anomalies at 700-mb height, contour interval 0.5 m s^{-1} and (b) meridional wintertime wind anomalies at 700-mb height, contour interval 0.5 m s^{-1} . Negative values are dashed. Shading indicates the regions where response is more than 95% significant.

exist the potential for the “delayed oscillator” mechanism in midlatitudes.

However, the question remains: How is this anomalous atmospheric circulation maintained? To address this issue, we diagnosed vorticity and thermodynamic budgets and came up with the physical mechanism described in the next section.

5. Physical mechanism

The anomalous heat fluxes at the surface themselves cannot explain the response of the large-scale atmospheric flow (Peng et al. 1997). Therefore, we analyzed the vorticity and thermodynamic budgets of the anomalous flow.

The vorticity and thermodynamic budgets were diagnosed based on the following equations:

$$u \frac{\partial \zeta}{\partial x} + v \frac{\partial \zeta}{\partial y} + \beta v = (\zeta + f) \frac{\partial \omega}{\partial p} + R$$

$$u \frac{\partial \theta}{\partial x} + v \frac{\partial \theta}{\partial y} + \omega \frac{\partial \theta}{\partial p} = Q,$$

where x is the horizontal coordinate in the longitudinal direction, y is the horizontal coordinate in latitudinal direction, p is the pressure, ζ is the relative vorticity, θ is the potential temperature, R is the vorticity forcing, and Q is the thermal forcing due to transient eddies (in a free atmosphere) and diabatic heating. The budgets

were calculated for each month separately for warm and cold cases (see Peng et al. 1997 for a detailed discussion on the calculation of these budgets), then averaged over 10 winters. As before, the results from the atmospheric cooling experiment were subtracted from the results of the heating experiment.

Figure 14 shows individual members of the vorticity balance at 700-mb height. The anomalous vorticity tendency due to the zonal advection (Fig. 14a) is weak. It is negative west of the date line and east of 150°W , and positive in the band between the date line and 150°W . Meridional advection (Fig. 14b) is significant in midlatitudes, but is also weak. In addition, meridional and zonal advections nearly compensate each other over two main regions of extrema. Thus the tendency due to horizontal advection is dominated by the tendency due to planetary vorticity advection βv (Fig. 14d). The anomalous vorticity tendency due to the divergence (Fig. 14c) is positive over the whole latitudinal belt between 20° and 45°N , and has a maximum at around 170°W . This maximum indicates the low-level convergence and ascent over this region. Comparison of (Figs. 14a–d) reveals that the anomalous vorticity balance north of 45°N is maintained by cancellation between the divergence term and the residual term that represents the tendency due to submonthly transient eddies (Fig. 14e). South of 45°N , the balance is between the same forcing except for additional vorticity advection contribution west of the date line. This balance is different from the balance

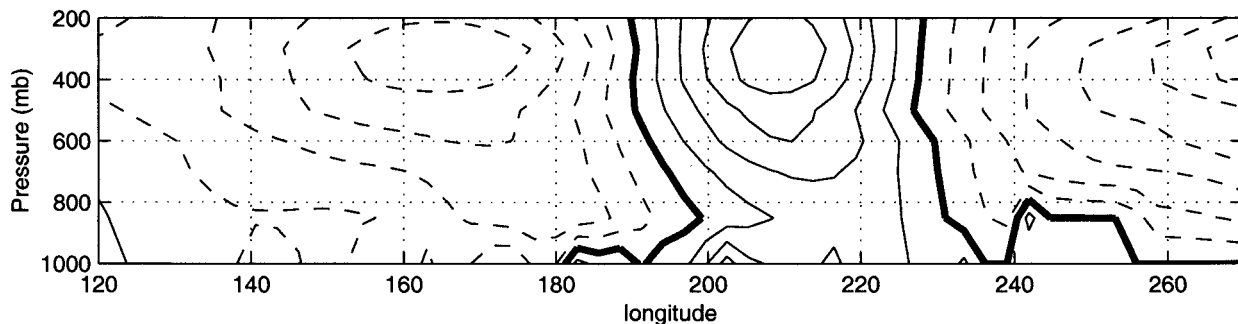


FIG. 12. Height–longitude cross section of the wintertime response in geopotential height at 40°N , contour interval 5 m.

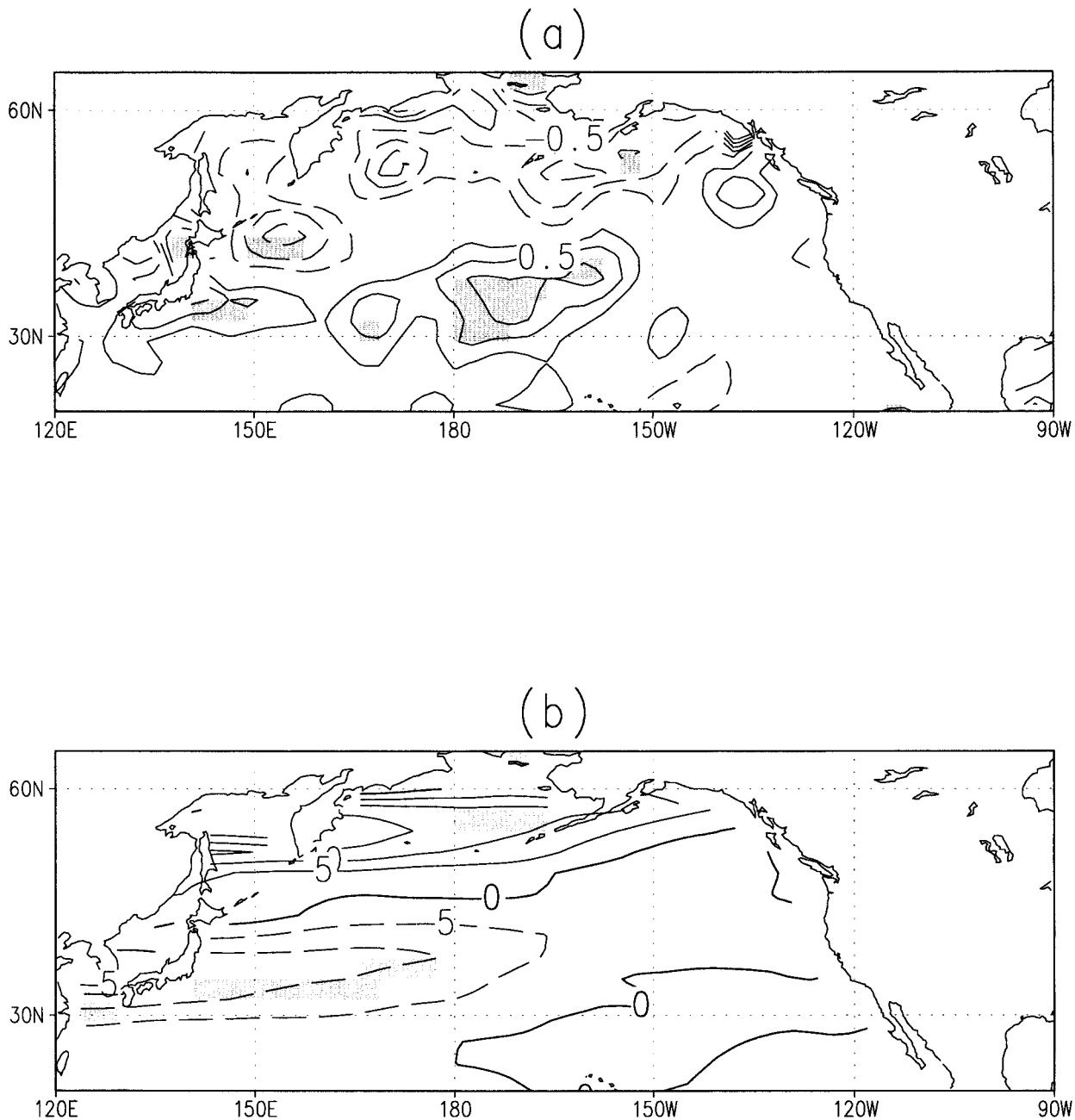


FIG. 13. (a) Ekman pumping velocity, interval 0.25 m s^{-1} , (b) Sverdrup transport, contour interval 5 Sv.

obtained by Hoskins and Karoly (1981) where the advection of planetary vorticity is balanced by downdraft into the heating region. Our balance is closer to the compensations presented by Peng et al. (1997) for their January case. The difference between the balance obtained in our studies and the balance in the linear primitive equation model (Hoskins and Karoly 1981) may be caused by the sensitivity of the response to the background state, location of the forcing relative to the storm track position (see Walter et al. 2001), the model's eddy

resolution, and the nonlinearity of the physical mechanism.

The anomalous temperature budget is shown in Fig. 15. At 700-mb height the radiative and turbulent mixing heating are smaller than convective and stratiform precipitation heating thus, diabatic heating (Fig. 15d) is represented by a sum of the last two components. In the steady state the tendencies due to zonal advection of temperature (Fig. 15a), vertical advection (Fig. 15c), and diabatic heating (Fig. 15d) are relatively small. Thus the

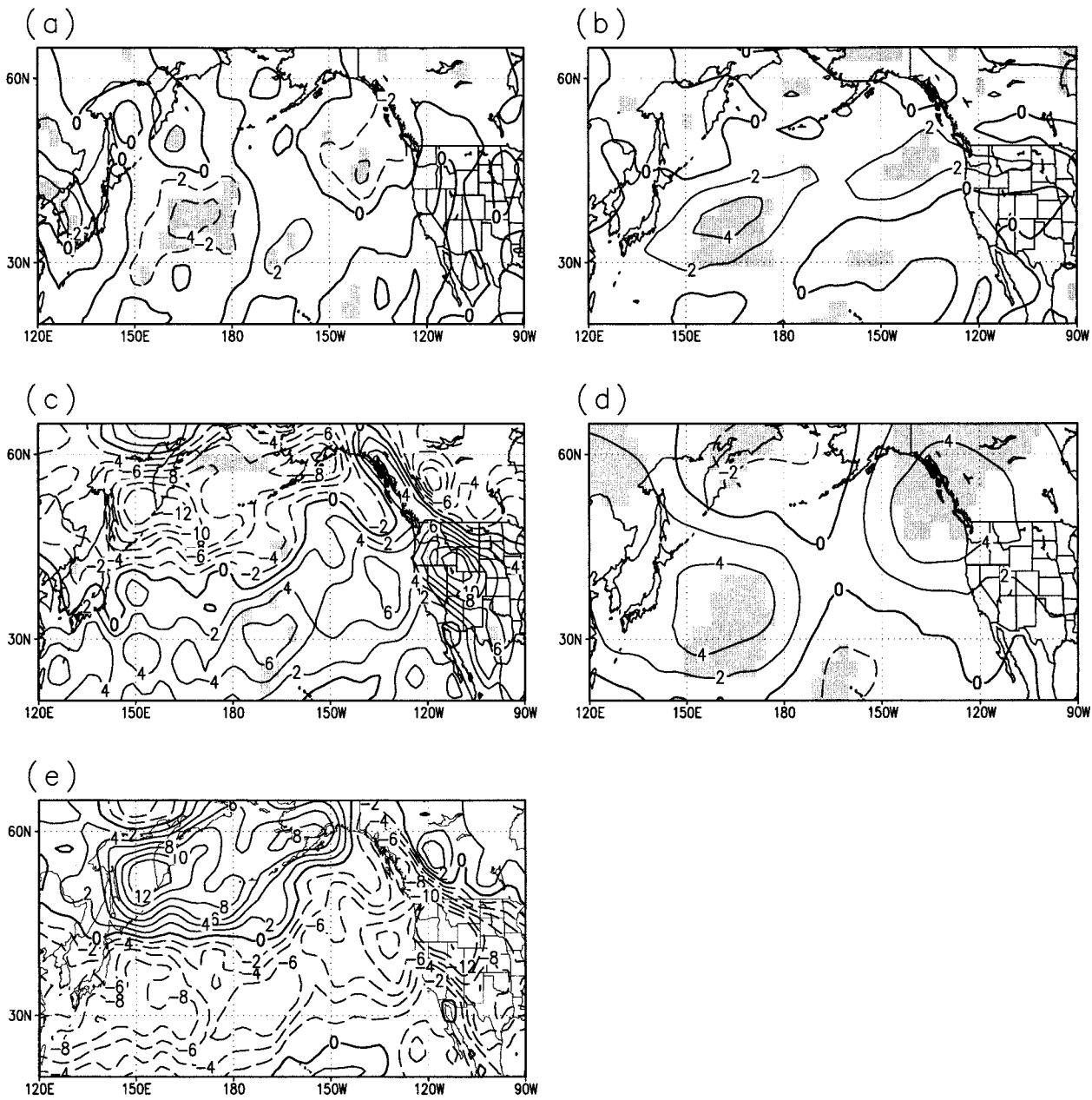


FIG. 14. Wintertime vorticity balance at 700 mb. Shading indicates the regions where response is more than 90% significant. Negative values are dashed. (a) Tendency due to zonal advection, contour interval $2 \times 10^{-11} \text{ s}^{-2}$; (b) tendency due to meridional advection, contour interval $2 \times 10^{-11} \text{ s}^{-2}$; (c) tendency due to divergence, contour interval $2 \times 10^{-11} \text{ s}^{-2}$; (d) tendency due to planetary vorticity advection, contour interval $2 \times 10^{-11} \text{ s}^{-2}$; (e) residual representing submonthly transient eddies, contour interval $2 \times 10^{-11} \text{ s}^{-2}$.

main balance is between the tendency due to the forcing by the residual transient eddies (Fig. 15e) and by the tendency due to meridional advection (Fig. 15b). The residual anomalous forcing (Fig. 15e) exhibits a pattern that is tilted to the northwest.

As was noted by Peng et al. (1997), the spatial structure of the thermal meridional advection can be explained by changes of the wind pattern downstream of the heating. The analysis of anomalous wind fields (Fig.

11b) exhibits the weakening of the meridional wind north of 30°N west of the date line that leads to weakening of the cold meridional advection downstream of the heating region. At the same time, the zonal jet stream intensifies east of the heating region (Fig. 11a) and can theoretically modify the transient eddy fluxes so that they reinforce the geopotential ridge required for additional cold advection.

In short, vorticity and thermodynamics budgets pre-

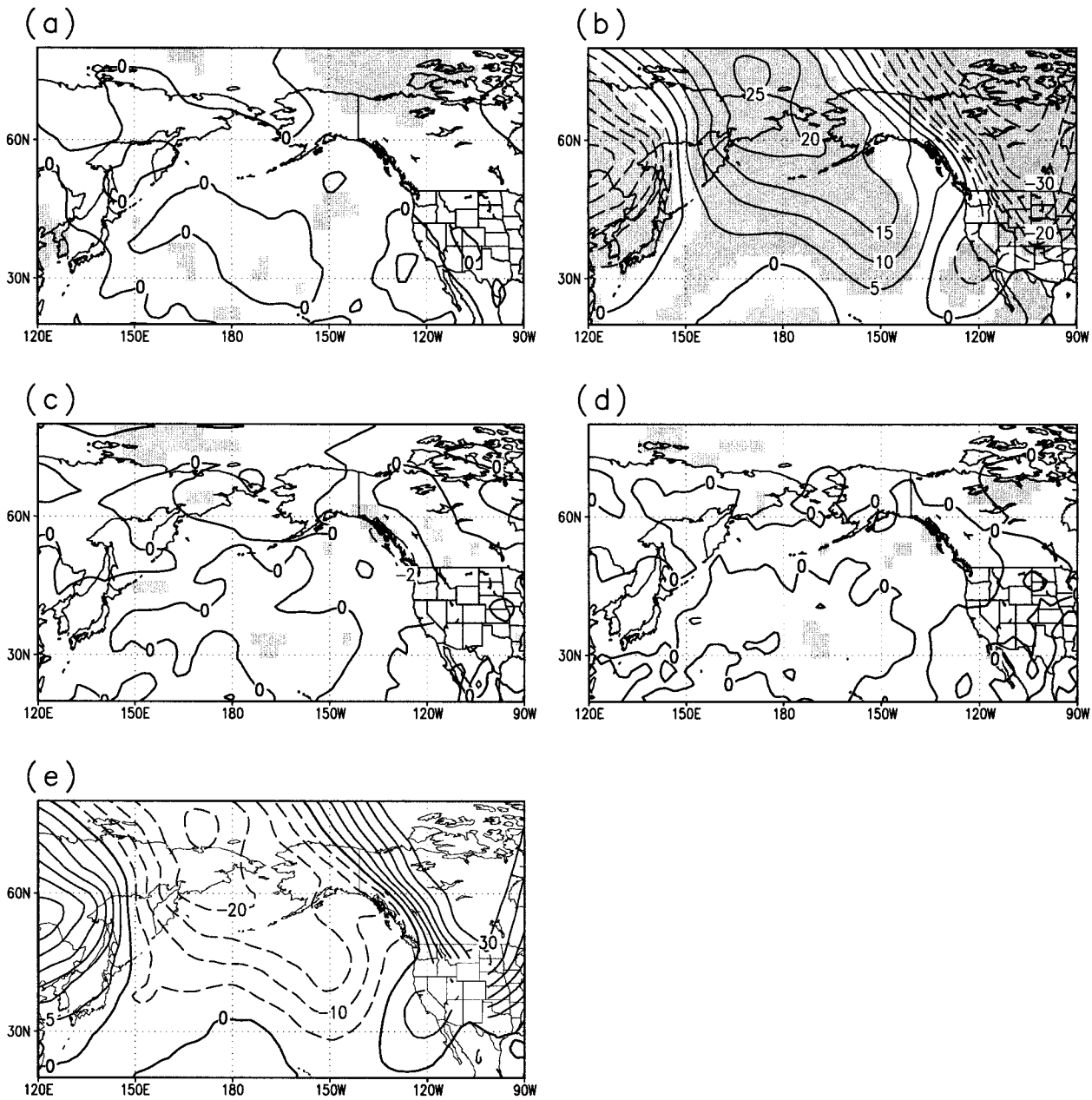


FIG. 15. Wintertime thermodynamic balance at 700-mb height, contour interval $5 \times 10^{-5} \text{ K s}^{-1}$. Shading indicates the regions where response is more than 90% significant. Negative values are dashed. (a) Tendency due to zonal advection; (b) tendency due to meridional advection; (c) tendency due to vertical advection; (d) tendency due to diabatic heating; (e) residual representing submonthly transient eddies.

sented in this section illustrate that submonthly transient eddies play a crucial role in maintaining the simulated atmospheric response. The eddy fluxes are most likely modified by the changes in the zonal jet stream exit that are determined by the amplitude and location of the oceanic forcing.

6. Summary and conclusions

In this study of the physical mechanism of climate variability in the North Pacific, we hypothesized that

upper-ocean heat fluxes perturbations are not influenced directly by stochastic atmospheric perturbations but rather represent the predictable aspect of low-frequency variability. Considering SST anomalies to be a part of the response of the coupled system, rather than the boundary forcing, allowed us to resolve the problem of strong damping inherent in classic “AMIP-type” experiments.

In the framework of this hypothesis we studied two competing processes that may cause low-frequency variability in midlatitudes. The first mechanism includes

oceanic heat budget changes in the Tropics teleconnected into midlatitudes by some atmospheric processes. The second mechanism reflects the ocean–atmosphere interaction in the North Pacific. In the first model integration experiment, the anomalous oceanic mixed layer heat flux was prescribed in the central tropical Pacific. The second integration was forced by the anomalous oceanic heat flux located in the midlatitude western Pacific, in the Kuroshio–Oyashio extension region. In both experiments, two 10-yr runs with different signs of heating were performed; the response was defined as the difference between the wintertime (DJF) means of these two runs. The comparison of atmospheric reaction in midlatitudes to the forcing located in the Tropics and in Kuroshio extension region reveals that the responses differ significantly.

The response to the tropical forcing resembles the second mode of internal variability of the control run, that is, a familiar PNA pattern in the Z500 field and the corresponding second mode of the SST anomalies.

When the model is forced by the oceanic heat flux in midlatitudes, Z500 anomaly pattern resembles the mixture of the first (WP) and second (PNA) modes of the internal variability of the control run. This response is equivalent barotropic and is determined by the dynamics of the transient eddies. The spatial distribution of SST anomalies correlates with the second mode of internal variability of the control run.

The patterns and amplitudes of the SST response in the western North Pacific are different. However in both scenarios the SST anomalies in the KOE region change significantly. Thus SST anomalies alone cannot indicate the location of the low-frequency predictable forcing on the atmosphere. This result gives one more proof to the main hypothesis of the manuscript, that is, that expressing boundary forcing on the atmosphere by prescribing upper-ocean heat flux anomalies allows for better understanding of the physical mechanism of low-frequency variability in midlatitudes.

The results of the midlatitude experiment provide a consistent description of the roles that ocean and atmosphere play in the process of excitation and maintaining of low-frequency variability in midlatitudes. The atmospheric response to the perturbation of the oceanic heat fluxes in midlatitudes can be described as follows:

- ocean heating anomalies in the Kuroshio Current extension region partially increase SST anomalies over this region, and partially are vented into the atmosphere;
- the corresponding adiabatic heating in the atmosphere is not confined to the surface, but rather have a maximum at 850-mb height level;
- away from the surface the warming is shifted eastward (see Hoskins and Karoly 1981), and horizontal advection is trying to balance it;
- the zonal advection is negligible in the steady state;
- the warming is balanced mainly by the cold advection

by the climatological meridional wind and by the transient eddies;

- the changes in the meridional wind require modification of geopotential height field to provide additional temperature advection;
- the resulting perturbations of the geopotential height are reinforced by transient eddy fluxes due to changes in the strength of the zonal winds at the jet exit (as was suggested by Ting and Peng 1995);
- the transient eddy fluxes lead to the change in the vorticity budget (as described in Hoskins and Karoly 1981), which implies the surface trough to the east of the heating region;
- the surface trough changes the wind stress field increasing cyclonic flow.

Though the oceanic dynamics is not included into the model, the analytical calculation of the Ekman transport divergence from the wind stress pattern qualitatively offers the “missing link” in the ocean–atmosphere interaction we explored. The corresponding Ekman pumping would decrease the Sverdrup transport into the forcing region, thus causing the cooling in the Kuroshio Current extension region. Therefore, the response in the atmospheric wind stress field in this region is consistent with the previously hypothesized low-frequency variability evolution in midlatitudes; it is in the sense that would be expected to change the oceanic state in the way that reduces the initial perturbation. This phenomenon resembles the “delayed oscillator” mechanism of decadal variability proposed by Latif and Barnett (1994, 1996) and Barnett et al. (1999). The crucial part of it implies the existence of the feedback path from the atmosphere into the ocean. The slow changes in the ocean to atmosphere heat flux alter the SST configuration and atmospheric dynamics not just locally but also globally; therefore they induce changes in the curl of the wind stress pattern. This anomalous wind curl alters Ekman pumping in the region of subtropical gyre in a way that counteracts the changes due to the oceanic heat fluxes. These changes in turn induce an opposite sign curl pattern, leading to the oscillation of the entire mechanism. The timescale of the oscillation induced by the mechanism described above is beyond the scope of this paper. Additional sets of experiments with realistically varying in time oceanic mixed layer heat fluxes are needed. On the other hand, the response in the region of the subpolar gyre acts in the opposite direction. If the heat transport of the subpolar gyre dominates, the warm SST anomalies in the Kuroshio extension region will be intensified and an additional mechanism will be required to explain the oscillatory low-frequency behavior.

The biggest caveat of the approach described in this paper consists in the absence of the oceanic dynamics, specifically in the absence of the Ekman advection that plays a significant role in maintaining SST anomalies pattern in the central North Pacific (Schneider et al. 2001, manuscript submitted to *J. Climate*). This dis-

advantage could be corrected in a few ways. The ocean dynamics must be included either implicitly by integrating fully coupled model, or explicitly by a “two-tier” integration. The first part of the two-tier approach involves simulation of the oceanic mixed layer heat flux anomalies by forcing an ocean general circulation model with observed or predicted atmospheric fluxes (wind stress). The next step consists of integrating an atmospheric GCM coupled to a Slab Ocean Model (with additional advection term) and forced with the obtained heat fluxes.

Another drawback consists in omitting the seasonal cycle of the surface heat budget perturbations. The oceanic heat anomalies in our simulations were considered to be constant in time while model simulations and observations reveal that the low-frequency variability is seasonally dependent. Introducing an annual cycle into prescribed forcing will correct this caveat. However, limiting the analysis to the winter season only allowed focusing on the time of the year when the atmosphere and ocean are coupled most efficiently and when the prescribed forcing qualitatively agrees with observations.

It should also be noted that the structure of atmospheric response in the midlatitude experiment might be determined by the spatial distribution of the anomalous forcing. In observations the low-frequency pattern of midlatitude SST anomalies is zonally elongated with local extrema in central and western North Pacific. Thus, this study should be followed by a detailed investigation of the sensitivity of the atmospheric response to the spatial structure of the forcing including a westward shift into the Kuroshio extension region.

In summary, the approach explored in this paper offers a consistent way of performing long-lead two-tier climate prediction over the North Pacific. It has a potential of increasing the skill of the interannual-to-decadal forecast over North America, and offers a new interpretation of the results from the previous long AMIP-type runs.

Acknowledgments. We gratefully acknowledge the help of Mary Tyree who executed the long control run of CCM3 coupled to SOM. This work was supported by Experimental Climate Prediction Center (ECPC) under NOAA NA77RJ0453, by the National Science Foundation (OCE97-11265), by Department of Energy’s CCPP Program, and by the Scripps Institution of Oceanography. The simulations were supplemented with the runs at the National Research Computing Center (NERSC) and NCAR’s Scientific Computing Division (SCD). We also thank Dr. R. Saravanan for valuable discussions and two anonymous reviewers for their important comments.

REFERENCES

- Alexander, M. A., 1992: Midlatitude atmosphere–ocean interaction during El Niño. Part II: The Northern Hemisphere atmosphere. *J. Climate*, **5**, 959–972.

- , and J. D. Scott, 1997: Surface flux variability over the North Pacific and North Atlantic Oceans. *J. Climate*, **10**, 2963–2978.
- Barnett, T. P., D. W. Pierce, M. Latif, D. Dommengat, and R. Saravanan, 1999: Interdecadal interactions between the tropics and midlatitudes in the Pacific basin. *Geophys. Res. Lett.*, **26**, 615–618.
- Barsugli, J. J., and D. S. Battisti, 1998: The basic effects of atmosphere–ocean thermal coupling on midlatitude variability. *J. Atmos. Sci.*, **55**, 477–493.
- Bhatt, U. S., M. A. Alexander, D. S. Battisti, D. D. Houghton, and L. M. Keller, 1998: Atmosphere–ocean interaction in the North Atlantic: Near-surface climate variability. *J. Climate*, **11**, 1615–1632.
- Blade, I., 1997: The influence of midlatitude ocean–atmosphere coupling on the low-frequency variability of a GCM. Part I: No tropical SST forcing. *J. Climate*, **10**, 2087–2106.
- Bretherton, C. S., and D. S. Battisti, 2000: An interpretation of the results from atmospheric general circulation models forced by the time history of the observed sea surface temperature distribution. *Geophys. Res. Lett.*, **27**, 767–770.
- Cayan, D. R., 1992: Latent and sensible heat flux anomalies over the northern oceans: The connection to monthly atmospheric circulation. *J. Climate*, **5**, 354–369.
- Deser, C., M. A. Alexander, and M. S. Timlin, 1999: Evidence for a wind-driven intensification of the Kuroshio Current Extension from the 1970s to the 1980s. *J. Climate*, **12**, 1697–1706.
- Frankignoul, C., and K. Hasselmann, 1977: Stochastic climate models. Pt. 2: Application to sea surface temperature anomalies and thermocline variability. *Tellus*, **29**, 289–305.
- Gershunov, A., and T. P. Barnett, 1998: Interdecadal modulation of ENSO teleconnections. *Bull. Amer. Meteor. Soc.*, **79**, 2715–2725.
- Hasselmann, K., 1976: Stochastic climate models. Pt. 1: Theory. *Tellus*, **28**, 473–485.
- Hoskins, B. J., and D. J. Karoly, 1981: Steady linear response of a spherical atmosphere to thermal and orographic forcing. *J. Atmos. Sci.*, **38**, 1179–1196.
- Hurrell, J. W., J. J. Hack, B. A. Boville, D. L. Williamson, and J. T. Kiehl, 1998: The dynamical simulation of the NCAR Community Climate Model Version 3 (CCM3). *J. Climate*, **11**, 1207–1236.
- Kalnay, E., and Coauthors, 1996: The NCEP/NCAR 40-Year Reanalysis Project. *Bull. Amer. Meteor. Soc.*, **77**, 437–471.
- Kiehl, J. T., J. J. Hack, G. B. Bonan, B. A. Boville, D. L. Williamson, and P. J. Rasch, 1998: The National Center for Atmospheric Research Community Climate Model: CCM3. *J. Climate*, **11**, 1131–1149.
- Kushnir, Y., and J. M. Wallace, 1989: Interaction of low- and high-frequency transients in a forecast experiment with a general circulation model. *J. Atmos. Sci.*, **46**, 1411–1418.
- , and N. C. Lau, 1992: The general circulation model response to a North Pacific SST anomaly: Dependence on time scale and pattern polarity. *J. Climate*, **5**, 271–283.
- , and I. M. Held, 1996: Equilibrium atmospheric response to North Atlantic SST anomalies. *J. Climate*, **9**, 1208–1220.
- Latif, M., and T. P. Barnett, 1994: Causes of decadal climate variability over the North Pacific and North America. *Science*, **266**, 634–637.
- , and —, 1996: Decadal climate variability over the North Pacific and North America: Dynamics and predictability. *J. Climate*, **9**, 2407–2423.
- Lau, N. C., and M. Nath, 1994: A modeling study of the relative roles of tropical and extratropical SST anomalies in the variability of the global atmosphere–ocean system. *J. Climate*, **7**, 1184–1207.
- , and —, 1996: The role of the “atmospheric bridge” in linking tropical Pacific ENSO events to extratropical SST anomalies. *J. Climate*, **9**, 2036–2057.
- Levitus, S., 1982: *Climatological Atlas of the World Ocean*. NOAA Professional Paper 13, 173 pp.
- Livezey, R. E., and T. M. Smith, 1999: Covariability of aspects of

- North American climate with global sea surface temperatures on interannual to interdecadal timescales. *J. Climate*, **12**, 289–302.
- Mehta, V. M., M. J. Suarez, J. Manganello, and T. L. Delworth, 2000: Oceanic influence on the North Atlantic Oscillation and associated Northern Hemisphere climate variations: 1959–1993. *Geophys. Res. Lett.*, **27**, 121–124.
- Miller, A. J., and N. Schneider, 2000: Interdecadal climate regime dynamics in the North Pacific Ocean: Theories, observations and ecosystem impacts. *Progress in Oceanography*, Vol. 47, Pergamon, 2–4.
- , D. R. Cayan, T. P. Barnett, N. E. Graham, and J. M. Oberhuber, 1994: Interdecadal variability of the Pacific Ocean: Model response to observed heat flux and wind stress anomalies. *Climate Dyn.*, **9**, 287–302.
- Palmer, T. N., and Z. Sun, 1985: Modeling and observational study of the relationship between sea surface temperature in the north-west Atlantic and the atmospheric general circulation. *Quart. J. Roy. Meteor. Soc.*, **111**, 947–975.
- Peng, S., and J. S. Whitaker, 1999: Mechanisms determining the atmospheric response to midlatitude SST anomalies. *J. Climate*, **12**, 1393–1408.
- , W. A. Robinson, and M. P. Hoerling 1997: The modeled atmospheric response to midlatitude SST anomalies and its dependence on background circulation states. *J. Climate*, **10**, 971–987.
- Pierce, D. W., 1996: *The Hybrid Coupled Model, Version 3: Technical Notes*. Scripps Institution of Oceanography Reference Series, No. 96-27, 66 pp.
- , T. P. Barnett, N. Schneider, R. Saravanan, D. Dommennget, and M. Latif, 2001: The role of ocean dynamics in producing decadal climate variability in the North Pacific. *Climate Dyn.*, in press.
- Pitcher, E. J., M. L. Blackmon, G. T. Bates, and S. Munoz, 1988: The effect of North Pacific sea surface temperature anomalies on the January climate of a general circulation model. *J. Atmos. Sci.*, **45**, 173–188.
- Rodwell, M. J., D. P. Rowell, and C. K. Folland, 1999: Oceanic forcing of the wintertime North Atlantic Oscillation and European climate. *Nature*, **398**, 320–323.
- Saravanan, R., 1998: Atmospheric low-frequency variability and its relationship to midlatitude SST variability: Studies using the NCAR Climate System Model. *J. Climate*, **11**, 1386–1404.
- , and P. Chang, 1999: Oceanic mixed layer feedback and tropical Atlantic. *Geophys. Res. Lett.*, **26**, 3629–3632.
- Schneider, N., A. J. Miller, and D. W. Pierce 2001: Anatomy of North Pacific decadal variability. *J. Climate*, submitted.
- Spiegel, M., 1991: *Theory and Problems of Statistics*. Schaum's Outline Series, McGraw-Hill, 504 pp.
- Ting, M., and S. Peng, 1995: Dynamics of the early and middle winter atmospheric responses to the northwest Atlantic SST anomalies. *J. Climate*, **8**, 2239–2254.
- Wallace, J. M., and D. S. Gutzler, 1981: Teleconnections in the geopotential height field during the Northern Hemisphere winter. *Mon. Wea. Rev.*, **109**, 784–812.
- , C. Smith, and Q. Jiang, 1990: Spatial patterns of atmosphere–ocean interaction in the northern winter. *J. Climate*, **3**, 990–996.
- Walter, K., U. Luksch, and K. Fraedrich, 2001: A response climatology of idealized midlatitude thermal forcing experiments with and without a storm track. *J. Climate*, **14**, 467–484.
- Xie, S.-P., T. Kunitani, A. Kubokawa, M. Nonaka, and S. Hosoda, 2000: Interdecadal thermocline variability in the North Pacific for 1958–97: A GCM simulation. *J. Phys. Oceanogr.*, **30**, 2798–2813.